The Effect of Zero-Net-Mass-Flux Jet Geometry on Active Separation Control of a NACA 0015 Airfoil

Trevor Stephens, Callum Atkinson and Julio Soria

Laboratory for Turbulence Research in Aerospace and Combustion, Monash University (Clayton Campus), Melbourne, VIC, 3800, Australia

Abstract. This paper reports on an experimental study that investigated the effect of geometry of zero-net-mass-flux (ZNMF) jets on the control of aerodynamic separation of a NACA 0015 airfoil over a range of angles of attack. In this investigation ZNMF jets of different geometries located at the leading edge of a NACA 0015 have been used to control boundary layer separation due to increasing angle of attack. The experiments reported in this paper were conducted in the 500 mm closed circuit water tunnel at the Laboratory for Turbulence Research for Aerospace & Combustion at Monash University. Three ZNMF jet geometries were considered - one was the 2D slot of height 0.15 mm spanning 500 mm of the airfoil investigated by [16] and two had an array of 1 mm diameter holes with varying pitch: (1) 1.7 mm pitch, 265 holes with a P/D = 1.7; (2) 6 mm pitch, 76 holes with a P/D = 6.0. Except for the results of the 2D slot control, all experiments were conducted at Re = 67,500, based on the chord of the airfoil. The forcing oscillations for the generation of the ZNMF jets were supplied by a 20 mm diameter piston/cylinder arrangement that was driven by a computer-controlled stepper motor via a Scotch-Yoke mechanism. The frequency of the oscillations was controllable by altering the rotational speed of the stepper motor, whilst the magnitude of the oscillations was adjusted by varying the crank length of the Scotch-Yoke mechanism. High spatial resolution Multigrid cross-correlation DPIV meaurements were undertaken in addition to force measurements and flow visualisations.

Key words: flow control, separation, wings, PIV.

1. Introduction

The use of passive flow control devices such as vortex generators and strakes has been used in the commercial aviation industry. These fixed objects have the disadvantage of creating unwanted parasitic drag when they are not required. Active flow control refers to techniques where energy is expended to modify the flow [3] and often involves replacing the fixed surfaces used in passive flow control with a series of jets intended to manipulate the fluid within the boundary layer. Its main advantage is that it can be "switched on" when required. One promising implementation involves using zero-net-mass-flux (ZNMF) jets [15, 16].

ZNMF jets are created from the working fluid of the flow system in which they are deployed, and thus transfer linear momentum without net mass injection into the system [8, 1, 2]. In the case of round ZNMF jets in cross-flow as used in this study, they are created from the periodic formation of vortex rings [5, 4].

An airfoil with ZNMF jet active flow control can be characterised by two non-dimensional parameters: The non-dimensional excitation frequency

$$F^+ \equiv \frac{fc}{U_\infty} \tag{1}$$

and the oscillatory momentum blowing coefficient

$$c_\mu \equiv \frac{J}{qc} = 2\frac{\overline{h}}{c}\left(\frac{U_{j\,rms}}{U_\infty}\right)^2 \quad . \tag{2}$$

The geometry of the row of circular jet orifices used in this study was expressed as the pitch to diameter ratio, P/D, defined in Fig. 1b. The effect of the P/D of dual circular ZNMF jets on their propagation in still air has been previously investigated [18]. The ZNMF jets in that study had $P/D = 5.71$ and 1.71, and different modes of propagation were identified for each case. For the wider spacing, the jets were unaffected by one another but when the spacing was reduced, the jets almost immediately combined into a single, larger jet, indicating that jet interaction depends on P/D.
Previous studies of ZNMF jets in flow control focused on two-dimensional jets [15, 16]. The effect on lift of this control approach and the corresponding flow visualistion is shown in Fig 1. However, a continuous slot along the leading edge of an aircraft has serious structural wing implications. The motivation for this study was to investigate the relationship between ZNMF jet geometry and the effectiveness of active flow control [14].

2. Experimental Apparatus and Methodology

2.1. Water tunnel, Airfoil and ZNMF Jet Control System

The experiments reported in this paper were conducted in the water tunnel at the Laboratory for Turbulence Research for Aerospace & Combustion at Monash University shown schematically in Figs 2 (a) and (b). This is a closed circuit, horizontal facility with five 1000 mm long working sections, each of 500 $mm \times 500$ mm cross-section. Flow uniformity is achieved with a perforated stainless steel plate, a honeycomb and a series of stainless steel screens in the settling chamber. The perforated plate (5 mm hole size with a 23% open area ratio) is placed immediately after the spray system followed by four screens of decreasing mesh size in the streamwise direction. The honeycomb section (12 mm diameter cell size and 120 mm cell length) is inserted between the first and second screens to straighten the flow and remove any mean swirl. A 10:1 contraction is used prior to the first working section to further reduce the turbulence intensity by accelerating the mean flow.
A maximum flow speed of 775 mm/s is achievable in the working sections with the current 53 kW AC motor and the in-line centrifugal pump system. The turbulence intensity level in the core region of the working section is less than 0.35%. The motor-pump system speed is controlled with an ABB Sami GS frequency controller which allows incremental steps in tunnel speed of $1\,mm/s$ over the entire flow speed range. A plenum chamber attached to the final working section diffuses the flow and returns it via a 300 mm diameter pipe to the pump. Perforated stainless steel plates in the plenum chamber (10 mm hole size with a 40% open area ratio), placed vertically and parallel to the working section walls, ensure minimal disturbance to the upstream working section flow while effectively redirecting the flow through 180° into the return pipe. A diatomaceous earth pool filter system running in parallel with the main return flow pipe-work removes contaminants from the water down to

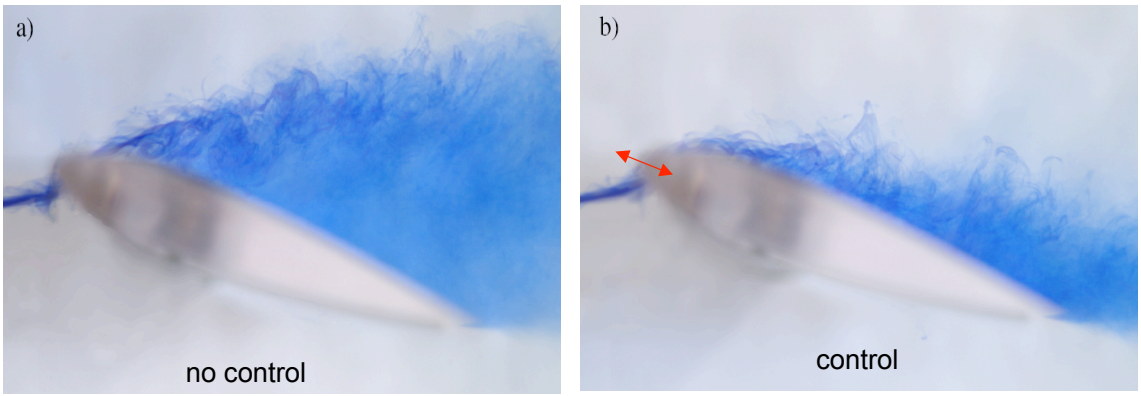

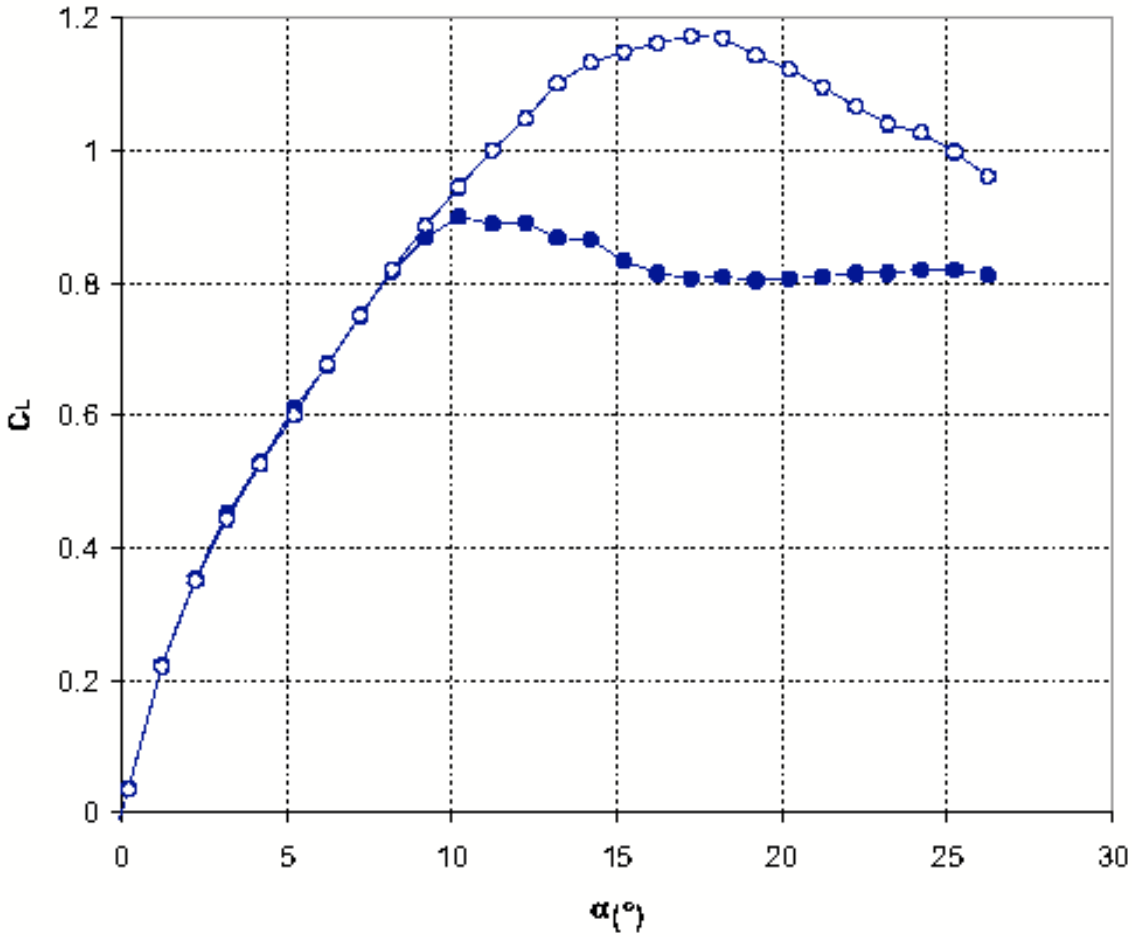

(c)

Figure 1. Die streak flow visualisations of a NACA 0015 airfoil at $Re = 3\times10^4 (Re_\theta = 600)$ and $\alpha = 18°$. (a) uncontrolled; (b) controlled. (c) C_L versus α for $Re = 3\times10^4 (Re_\theta = 600)$, $c_\mu = 0.14\%$ and $F^+ = 1.3$ - filled circles = uncontrolled, unfilled circles = controlled flow [15].

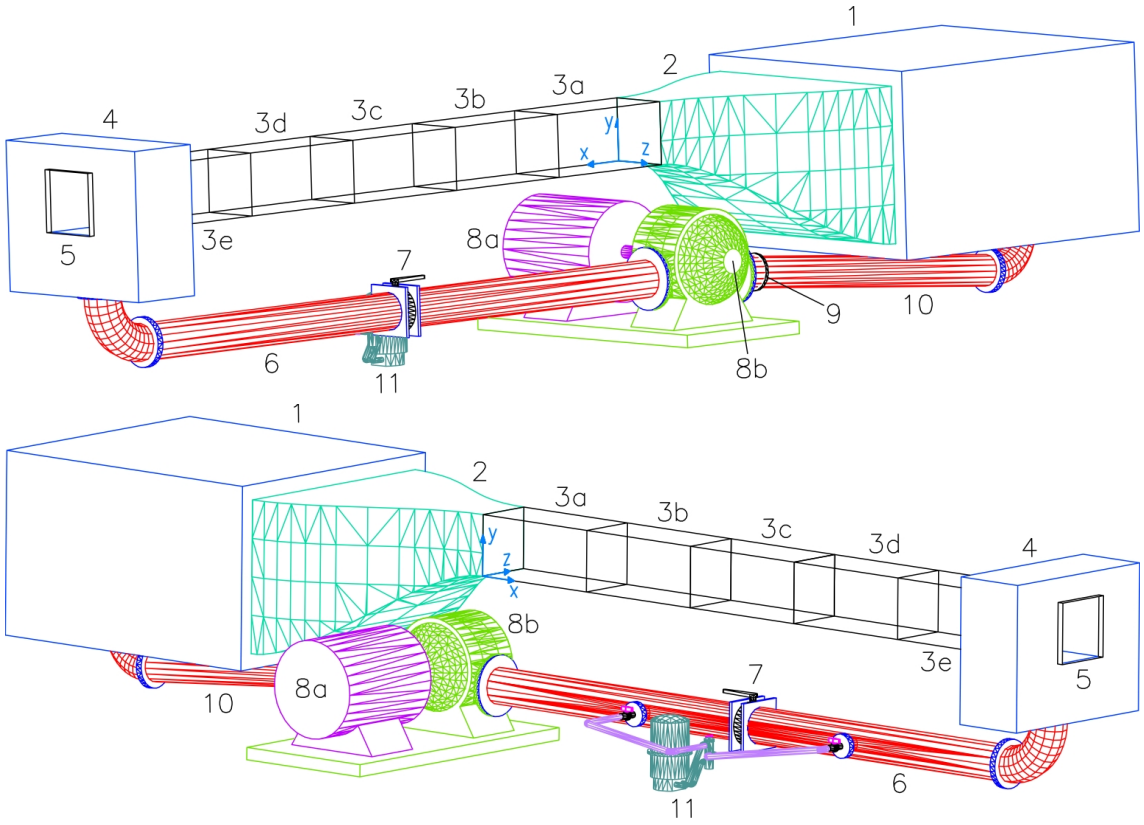

Figure 2. SCHEMATIC OF LTRAC 500 $mm \times 500$ mm WATER TUNNEL.

Table 1. Specifications of the NACA 0015 airfoils used in this investigation

P/D	n	A_j (mm^2)	b_n (mm)	$\overline{h}$ (mm)
6.0	76	59.69	456.0	0.1309
1.7	265	208.13	450.5	0.4620

a level of 5 μm. The filtration can be activated at any time, but it is never operated during experiments.

Two NACA 0015 airfoils with 150 mm chord and 510 mm span were manufactured for this study. The airfoils were mounted vertically, through a rotation stage, to a six-component force transducer which measured lift forces at 21.33 Hz with a resolution of 0.116 N or $\Delta C_L \approx 0.025$. Force data was acquired for 4 minutes or 5120 samples for each test condition. Analysis of force transducer data found that the error from the transducer's operation and the aerodynamic force fluctuations was $\Delta C_{L\,20} \approx 2\%$.

Rows of 1 mm diameter, surface normal holes were machined along the leading edges with $P/D = 6.0$ and 1.7; equivalent to the values used by [18]. The holes were fed by a 6 mm diameter cavity inside the leading edge of the airfoil, as shown in Fig. 3 (a), through which flow oscillations were supplied to generate a row of ZNMF jets. The flow oscillations were supplied by a 20 mm diameter piston driven by a computer controlled stepper motor via a Scotch-Yoke mechanism. Table 1 lists the specifications of the two airfoils.

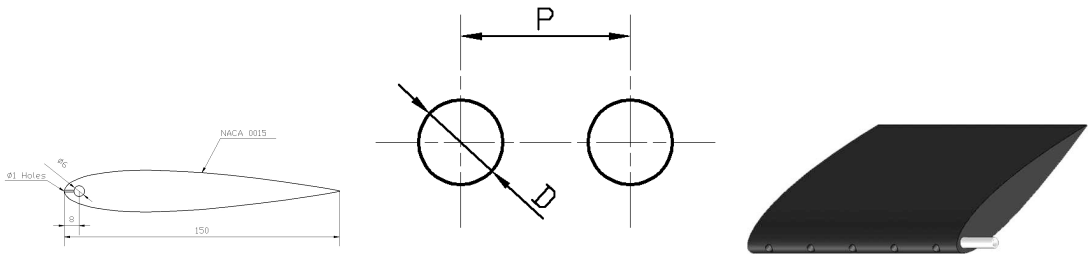

(a) (b) (c)

Figure 3. Drawings of the NACA 0015 airfoils (a, c) and ZNMF jet geometry (b)

2.2. Multigrid Cross-correlation Digital PIV

Prior to the PIV experiments, the flow was uniformly seeded with approximately neutrally bouyant hollow glass spheres, which have a nominal diameter of 11 μm with a density of 1100 kg/m^3 and a particle relaxation time of 9 μs. The illumination source for the recording of PIV images is a New Wave Nd:YAG twin cavity laser system capable of producing 2 $\times$ 200 mJ pulses of 6 ns duration at 15 Hz. A cylindrical lens was used to expand the laser beam into a sheet 2 mm thick. The laser sheet bisected the width of the NACA 0015 airfoil.
The scattered light from the seed particles was recorded on a monochrome PCO pco.4000 14 bit digital CCD camera with array size 4008 px $\times$ 2672 px. This digital camera can be operated in double shutter mode for single exposed PIV image recording. A 105 mm Micro-Nikkor lens set at an aperture of $f2.8$ and a reproduction ratio of approximately 8 was used for all experiments. The spatial resolution used was 56.25 μm/pixel.
The single exposed image pairs were analyzed using the multigrid cross-correlation digital particle image velocimetry (MCCDPIV) algorithm described in [13], which has its origin in an iterative and adaptive cross-correlation algorithm introduced by [9, 11, 10]. Details of the performance, accuracy and uncertainty of the MCCDPIV algorithm with applications to the analysis of single exposed PIV and holographic PIV (HPIV) images have been reported in [12] and [17] respectively.
The present single exposed image acquisition experiments were designed for a two-pass MCCDPIV analysis. The first pass used an IW = 64 px, while the second pass used an IW = 32 px with discrete IW offset to minimize the measurement uncertainty [20]. The sampling spacing between the centres of the IW was 16 px.
The MCCDPIV algorithm also uses the local cross-correlation function multiplication method introduced by [6] to improve the search for the location of the maximum value of the cross-correlation function. For the sub-pixel peak calculation, a two dimensional Gaussian function model was used to find, in a least square sense, the location of the maximum of the cross-correlation function [9].
The MCCDPIV data field was subsequently validated by using a combination of global histogram operator check [7], a median test [19] and the dynamic mean value operator test described in [7]. Following data validation, the in-plane velocity components (u, v) in the (x, y) coordinate directions respectively were computed by dividing the measured MCCDPIV displacement in each interrogation window by the time between the exposures of the image pair. The x coordinate direction is taken as the free-stream direction, while the y direction is the cross-stream direc-

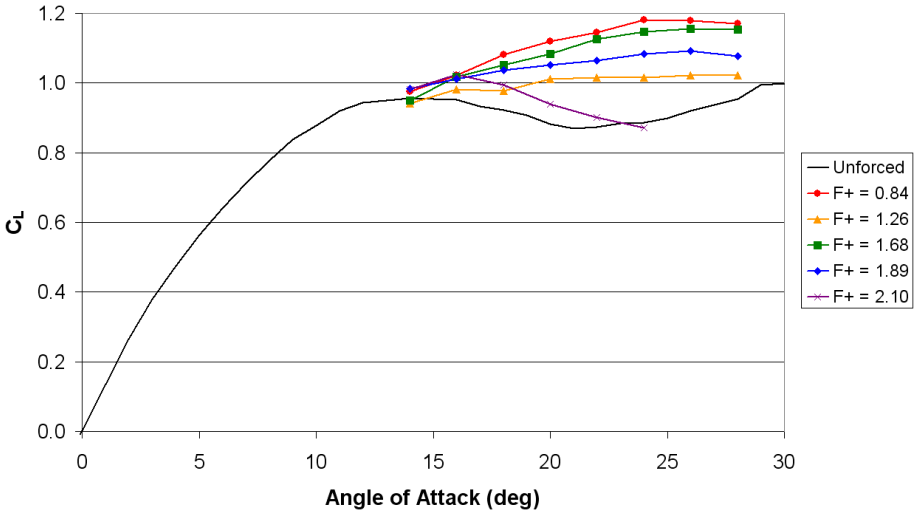

Figure 4. Sample of results for $c_\mu = 0.053\%$ at $Re = 6.56 \times 10^4$

tion. The uncertainty relative to the maximum velocity in the velocity components at the 95% confidence level for these measurements is 0.3%.
The out-of-plane vorticity, ω_z, was calculated from the MCCDPIV velocity field measurements using a local least-squares fit procedure to the velocity field, followed by analytic differentiation [11] using the relationship

$$\omega_z = \partial v/\partial x - \partial u/\partial y. \tag{3}$$

A thirteen point, two-dimensional, local fit to the data was used.
The final pass interrogation window size of 32×32 pixels yielded a 125×83 vector field. During the control experiments, phase locking was avoided by offsetting the optimum frequencies, multiples of 0.5 Hz, by 0.04 Hz. The 2 Hz acquisition frequency also ensured the statistical independence of each PIV image pair. 200 instantaneous vector fields were averaged to produce the time-averaged data.

3. Results

3.1. Force Measurements

The effect of changing the geometry of ZNMF jet orifices was investigated through a parametric force measurement study of each airfoil at the same conditions and comparing their behaviour at a Reynolds number of 6.56×10^4. The uncontrolled $C_{L\,Max}$ and $C_{L\,20}$ were measured for both airfoils. $C_{L\,Max}$ for both airfoils was found to occur at 16°. For $P/D = 6.0$, $C_{L\,Max} = 0.987$ and $C_{L\,20} = 0.911$ and for $P/D = 1.7$, $C_{L\,Max} = 0.981$ and $C_{L\,20} = 0.906$. These values are well within the experimental error of each other.
The dependence of the effectiveness of the active flow control on F^+ and c_μ was investigated. This was evaluated by holding c_μ constant and varying F^+ from 0.42 to 2.11. The first stages of this investigation aimed to find the angle of attack, if one existed, at which a controlled airfoil would reach its maximum lift coefficient. Figure 4 shows a sample result for this investigation.

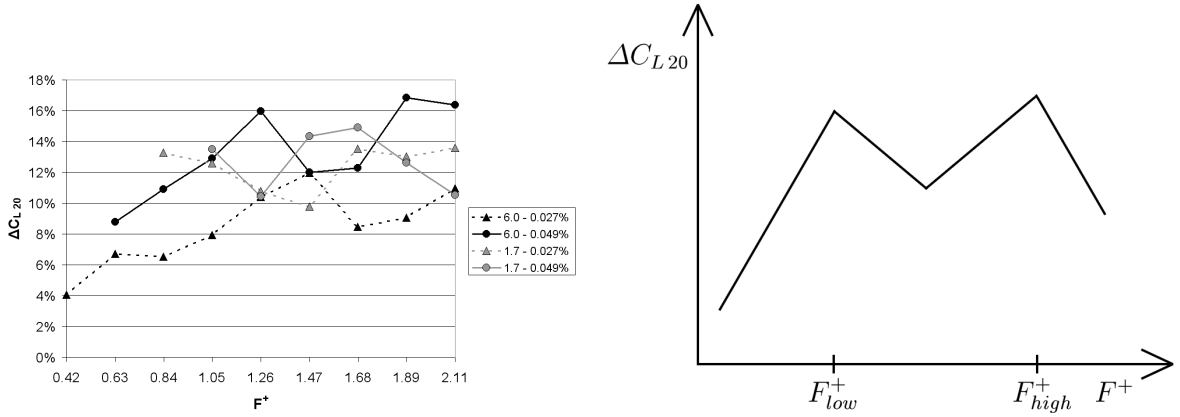

(a) (b)

Figure 5. $\Delta C_{L\,20}$ as a function of F^+ at $Re = 6.56 \times 10^4$ (a) and schematic of $\Delta C_{L\,20}$ curve shape (b)

A broad range of F^+ and c_μ were investigated in this manner with 2° steps in angle of attack. 44 different combinations of the ZNMF jet orifice P/D and the amplitude and frequency of oscillation were tested. For more than 90% of the test conditions examined, the controlled maximum lift angle was in the range of $20° \pm 2°$. Thus, a 20° angle of attack was used for all further work.

The effectiveness of the flow control was quantified as the percentage increase in lift at 20° and given the notation $\Delta C_{L\,20}$. Both airfoils were investigated in this way for the same range of F^+ previously examined at $c_\mu = 0.027\%$ and 0.049%. The dependence of c_μ on the experimental set up meant not all forcing frequencies could be investigated due to the piston displacement limits.

Figure 5 (a) shows the parametric study's results for both airfoils. The general shape of this percentage lift increase curve is similar for both airfoils with two peaks of high active flow control effectiveness at two frequencies, F^+_{low} and F^+_{high}. Between and on either side of these peaks, the effectiveness reduces. This is summarised in the schematic in Fig. 5 (b).

It is apparent that over some ranges of F^+, no lift increase due to increased c_μ is measured for the $P/D = 1.7$ case. The $P/D = 6.0$ case however shows a greater increase in control effectiveness over the entire spectrum of F^+ investigated. It was also observed that increasing c_μ appeared to shift the peak frequencies to slightly lower values.

For $c_\mu = 0.049\%$, the peak frequencies and their active flow control effectiveness are clearly different between the two different P/D cases. Table 2 summarises the important results at $c_\mu = 0.049\%$. This data indicates that the control effectiveness at F^+_{low} and F^+_{high} is similar, being within the experimental error. The worst performing P/D case was 1.7. It is possible that jet interaction differences, similar to those seen in [18], may have caused the reduced control effectiveness.

3.2. MCCDPIV

The conditions found to be optimal for control in the parametric study were investigated further with PIV at the same Reynolds number of 6.56×10^4. The F^+_{high} control frequencies were selected since the peaks were better resolved. In order to

Table 2. The effect of P/D on $\Delta C_{L\,20}$ at $c_\mu = 0.049\%$ and $Re = 6.56 \times 10^4$

P/D	F^+_{low}	$\Delta C_{L\,20}$	F^+_{high}	$\Delta C_{L\,20}$
6.0	1.26	16.0%	1.89	16.9%
1.7	1.05	13.5%	1.68	14.9%

obtain the maximum difference between the uncontrolled and controlled cases the angle of attack was reduced to 16° with $c_\mu = 0.049\%$.
Figure 6 shows time-averaged streamlines for the uncontrolled case and both controlled cases. The uncontrolled airfoil results show a large recirculating region on the suction side of the arifoil with its centre lying at approximately 80% chord. With control activated, the $P/D = 6.0$ case shows a drastically reduced recirculation region with smooth, attached flow pbserved for almost the entire chord. A very small recirculation region is present right at the trailing edge. The $P/D = 1.7$ result also shows a significant improvement. Reynolds stresses were also measured for these two cases and are reported in [14].

4. Concluding Remarks

The geometry of a row of round, wall-normal, ZNMF jets located at the leading edge of a NACA 0015 airfoil has been seen to effect the optimum frequencies of active flow control. These optimum frequencies were identified as $F^+ = 1.89$ for a row of jets with $P/D = 6.0$ and $F^+ = 1.68$ for $P/D = 1.7$ but were seen to rely on the c_μ at which the jets were operated. A second optimum frequency of similar effectiveness was seen at a lower frequency for each P/D case. The effectiveness of each was found to increase with increasing c_μ. The most effective P/D of the two was found to be 6.0. It is possible that differences in jet interaction mechanisms due to their geometry may have caused the different control effectiveness for each P/D case. Time-averaged streamlines indicate a reduction in the size of a recirculation region over the upper surface of the airfoil, likely to have caused the improved lift observed.

Acknowledgements

The authors would like to acknowledge the significant efforts of Dr. Kamal Parker and Ashley Tuck for setting up much of the apparatus adapted to this experiment, Eric Wirth and Ivor Little for manufacturing the apparatus used, Professor Bijan Shirinzadeh for the generous loan of the force transducer and the financial support of the ARC and AFOSR/AOARD.

References

[1] J. Cater, F. Bertillino, and J. Soria. Investigation of the far field of axisymmetric zero-net-mass flux jets using cross-correlation PIV. In J. Soria and D. Honnery, editors, *Proceedings of the Second Australian Conference on Laser Diagnostics in Fluid Mechanics and Combustion*, pages 144–149, Monash University, Melbourne, Australia, December 1999. Monash University Printing Services.

[2] J. Cater and J. Soria. The evolution of round zero-net-mass flux jets. *J. Fluid Mech.*, 472:167 – 200, 2002.

[3] J. F. Donovan, L. D. Kral, and A. W. Cary. Active flow control applied to an airfoil, 1998. AIAA Paper 0210.

[4] M. Gordon, J.E. Cater, and J. Soria. Investigation of the mean passive scalar field in zero-net-mass-flux in cross-flow using plif. *Phys. Fluids*, 16(3):794 – 808, 2004.

[5] M. Grodon and J. Soria. Piv measurements of a zero-net-mass-flux jet in cross flow. *Exp. Fluids*, 33:863 – 872, 2002.

[6] D.P. Hart. The elimination of correlation error in PIV processing. In *9^{th} International Symposium of Applications of Laser Techniques to Fluid Mechanics*, pages I:13.3.1 – 13.3.8, Lisbon, Portugal, July 1998.

[7] M. Raffel, C. Willert, and J. Kompenhans. *Particle Image Velocimetry.* Springer-Verlag, 1998.

[8] Barton L. Smith and A. Glezer. The formation and evolution of synthetic jets. *Phys. Fluids*, 10(9):2281–2297, September 1998.

[9] J. Soria. Digital cross-correlation particle image velocimetry measurements in the near wake of a circular cylinder. In *Int. Colloquium on* Jets, Wakes and Shear Layers, pages 25.1 – 25.8, Melbourne, Australia, 1994. CSIRO.

[10] J. Soria. An adaptive cross-correlation digital PIV technique for unsteady flow investigations. In A.R. Masri and D.R. Honnery, editors, *Proc. 1st Australian Conference on Laser Diagnostics in Fluid Mechanics and Combustion*, pages 29 – 48, Sydney, NSW, Australia, Dec 1996. University of Sydney, University of Sydney.

[11] J. Soria. An investigation of the near wake of a circular cylinder using a video-based digital cross-correlation particle image velocimetry technique. *Experimental Thermal and Fluid Science*, 12:221 – 233, 1996.

[12] J. Soria. Multigrid approach to cross-correlation digital PIV and HPIV analysis. In *13th Australasian Fluid Mechanics Conference*, pages 381–384, Monash University, Melbourne, 1998.

[13] J. Soria, J. Cater, and J. Kostas. High resolution multigrid cross-correlation digital PIV measurements of a turbulent starting jet using half frame image shift film recording. *Opt. Las. Technol.*, 31:3–12, 1999.

[14] T. Stephens. The effect of zero-net-mass-flux jet geometry on active flow control of a naca 0015 airfoil, 2006. Honours Thesis, Laboratory for Turbulence Research in Aerospace and Combustion (LTRAC), Department of Mechanical Engineering, Monash University, Melbourne, Australia.

[15] A. Tuck. Active flow control of a naca 0015 airfoil using a znmf jet, 2004. Honours Thesis, Laboratory for Turbulence Research in Aerospace and Combustion (LTRAC), Department of Mechanical Engineering, Monash University, Melbourne, Australia.

[16] A. Tuck and J. Soria. Active flow control over a naca 0015 airfoil using a znmf jet. In M. Behnia, W. Lin, and G. D. McBain, editors, *Fifteenth Australasian Fluid Mechanics Conference (CD-ROM)*. The University of Sydney, 2004.

[17] K. von Ellenrieder, J. Kostas, and J. Soria. Measurements of a wall-bounded turbulent, separated flow using HPIV. *Journal of Turbulence*, 2:1–15, 2001.

[18] M. Watson, A.J. Jaworski, and N.J. Wood. Contribution to the understanding of flow interactions between multiple synthetic jets. *AIAA Journal*, 41(4):747 – 749, 2003.

[19] J. Westerweel. Efficient detection of spurious vectors in particle image velocimetry data. *Exp. Fluids*, 16:236–247, 1994.

[20] J. Westerweel, D. Dabiri, and M Gharib. The effect of a discrete window offset on the accuracy of cross-correlation analysis of digital PIV recordings. *Expt. Fluids*, 23:20 – 28, 1997.

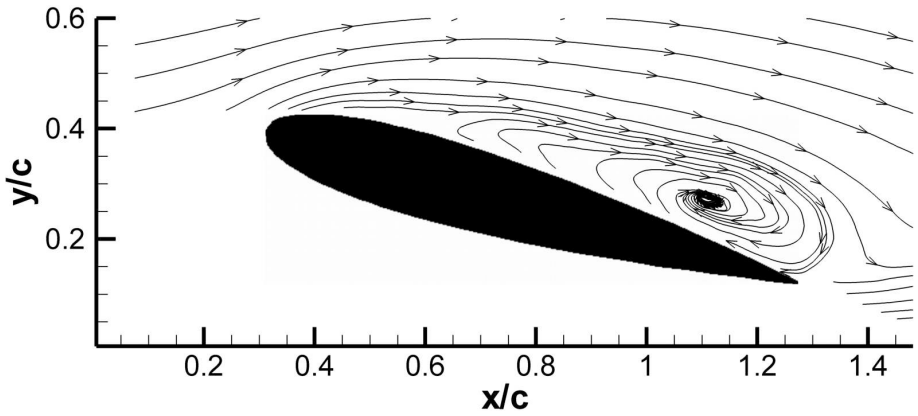

(a)

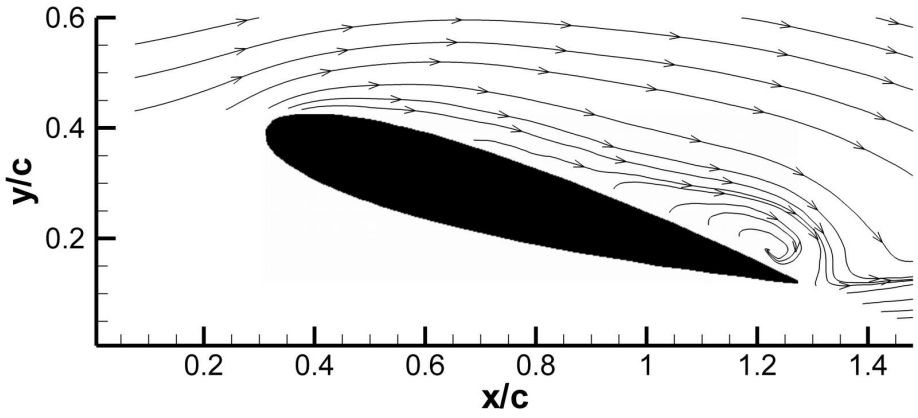

(b)

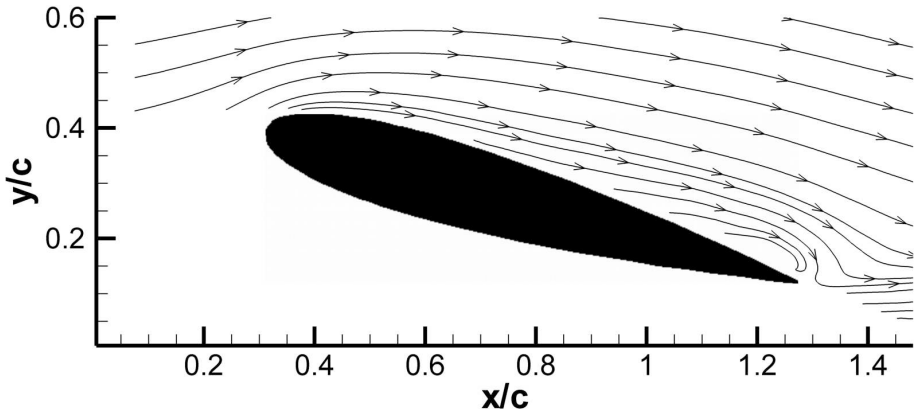

(c)

Figure 6. Time-averaged streamlines at $Re = 6.56 \times 10^4$ and $\alpha = 16^o$ for: (a) the uncontrolled airfoil; the controlled airfoil with $c_\mu = 0.049\%$ at F^+_{high} when (b) $P/D = 1.7$ and (c) when $P/D = 6.0$